


Lifetime measurements of short-lived excited states, and shape changes in ^{69}As and ^{66}Ge nuclei

M. Matejska-Minda ^{1,*}, P. Bednarczyk,¹ B. Fornal,¹ F. R. Xu,² W. Y. Liang,² G. de Angelis,³ S. Aydin,^{4,5} S. Brambilla,⁶ M. Ciemala,¹ E. Farnea,^{3,†} T. Hüyük,³ G. Jaworski,⁷ M. Kmiecik,¹ M. Krzysiek,¹ S. Leoni,^{6,8} A. Maj,¹ R. Menegazzo,⁴ W. Męczyński,¹ C. Michelagnoli,^{3,9} M. Palacz,⁷ F. Recchia,⁴ E. Sahin,^{3,10} J. Styczeń,¹ B. Szpak,¹ C. A. Ur,^{4,11} R. Wadsworth,¹² and M. Ziębliński¹

¹*Institute of Nuclear Physics Polish Academy of Sciences, PL-31342 Cracow, Poland*

²*School of Physics, Peking University, Beijing 100871, China*

³*INFN, Laboratori Nazionali di Legnaro, I-35020 Legnaro, Italy*

⁴*INFN, Sezione di Padova, I-35131 Padova, Italy*

⁵*Department of Physics, Aksaray University, Aksaray, Turkey*

⁶*INFN, Sezione di Milano, I-20133 Milano, Italy*

⁷*Heavy Ion Laboratory, University of Warsaw, PL-02093 Warsaw, Poland*

⁸*Dipartimento di Fisica, Università degli Studi di Milano, I-20133 Milano, Italy*

⁹*ILL, CS 20156, 38042 GRENOBLE Cedex 9 - France*

¹⁰*Department of Physics, University of Oslo, P.O. Box 1048, Blindern, N-0316 Oslo, Norway*

¹¹*IFIN-HH, P.O. BOX MG-6, Bucharest-Magurele, Romania*

¹²*Department of Physics, University of York, UK-YO10 5DD, United Kingdom*



(Received 1 July 2019; published 26 November 2019)

Background: The nuclear shape is a macroscopic feature of an atomic nucleus that is sensitive to the underlying nuclear structure in terms of collectivity and the interaction between nucleons. Therefore, the evolution of nuclear shapes has attracted many theoretical and experimental nuclear structure studies. The structure of the $A \approx 70$, $N \approx Z$ nuclei, lying far from the stability line, is interesting because a particularly strong proton-neutron correlation may occur here due to the occupation of the same orbits by nucleons of both types. In this region, different particle configurations drive a nucleus towards various deformed shapes: prolate, oblate, octupole, or nonaxial. These nuclear shapes change rapidly with nucleon number and also with angular momentum. This is reflected by a presence of different structures (bands) of excited states which exhibit a broad range of lifetimes.

Purpose: The aim of this paper is to determine lifetimes of some high-spin excited states in ^{69}As and ^{66}Ge nuclei to examine the shape evolution in these neutron-deficient nuclei.

Methods: Lifetimes of high-spin states in ^{69}As and ^{66}Ge have been measured by using the Doppler-shift attenuation technique with the GASP and recoil filter detector setup at the Laboratori Nazionali di Legnaro. The nuclei of interest were produced in the $^{32}\text{S}(95\text{ MeV}) + 0.8\text{ mg/cm}^2\text{ }^{40}\text{Ca}$ fusion-evaporation reaction. The strongest reaction channels $3p$ and $\alpha 2p$ led to the ^{69}As and ^{66}Ge final nuclei, respectively. Using γ - γ -recoil coincidences we were able to determine very short lifetimes (in the femtosecond range) in the residual nuclei of interest.

Results: In ^{69}As , the extracted lifetimes are $\tau = 72$ (-32 , $+45$) fs for the $33/2^+$ state at 7897 keV and $\tau < 85$ fs for the $37/2^+$ state at 9820 keV. For the ^{66}Ge case, the lifetime of the 11^- state at 7130 keV is $\tau = 122$ (± 41) fs. Lifetimes in ^{69}As and ^{66}Ge reported in this paper have been measured for the first time in the present experiment.

Conclusions: The results are discussed in the terms of deformation and shape evolution in ^{69}As and ^{66}Ge . The quadrupole moments deduced from the measured lifetimes were compared with the cranked Woods-Saxon-Strutinsky calculations by means of the total Routhian surface method. It turns out that *Band 3* in ^{69}As shows an oblate-prolate shape transition, and above spin $33/2^+$ it corresponds to a prolate collective structure with $\beta_2 \approx 0.27$ and $\gamma \approx 20^\circ$. In turn, in ^{66}Ge the negative-parity band built on the 7^- state at 4205 keV corresponds to a triaxial shape with $\beta_2 = 0.33$ and $\gamma = 31^\circ$. Analysis of the transitional quadrupole moments derived from the experimental and theoretical ones points to a significant change of deformation in the ^{69}As and ^{66}Ge nuclei with increasing rotational frequency.

DOI: [10.1103/PhysRevC.100.054330](https://doi.org/10.1103/PhysRevC.100.054330)

*Magdalena.Matejska-Minda@ifj.edu.pl

†Deceased.

I. INTRODUCTION

The neutron-deficient ^{69}As and ^{66}Ge nuclei lie close to the $N = Z$ line, between the doubly magic ^{56}Ni and strongly deformed ^{76}Sr nuclei. Species in that region are known to exhibit a variety of nuclear shapes, which can be attributed to large shell gaps at both prolate and oblate deformation for proton and neutron numbers $N, Z = 34, 36$ [1–3]. Nuclides in that region reveal shape instability that is manifested by a presence of rotational bands associated with moderate quadrupole deformation, $\beta_2 \approx 0.3$, and a significant degree of triaxiality. Coexistence of the prolate and oblate shapes is here a typical phenomenon.

The nuclear shape is a very sensitive probe of the underlying nuclear structure and the interaction between nucleons. Observables such as lifetimes, which give transition strengths between excited nuclear states and, consequently, information on the electric-quadrupole moment are important reference points for nuclear structure theory. They provide information on the properties of collective structures including nuclear deformation which for the nuclei of interest is still rather scarce. This is due to the limitations in measuring such short, femtosecond-range expected lifetimes.

To investigate experimentally the evolution of nuclear deformation in the $A \approx 70$, $N \approx Z$ region, we measured the lifetimes of excited states in the ^{69}As and ^{66}Ge nuclei produced in a fusion-evaporation reaction. To interpret the measured lifetimes and to draw conclusions about the underlying nuclear shapes, the results are compared with the outcome of the cranked Woods-Saxon-Strutinsky calculations by means of the total Routhian surface (TRS) method [4]. The preliminary results from this experiment, together with a theoretical interpretation, have been reported elsewhere [5,6]. A variety of nuclear shapes is expected in the $A \approx 70$ nuclei. Therefore, this region constitutes an interesting playground for studies of shape evolution and shape coexistence, both in theory and experiment, and prompted several recent investigations; see, e.g., Refs. [7–12]. In these studies, the results of theoretical calculations are compared with the experimental level schemes and kinematic or dynamic moments of inertia are deduced. In the present paper, conclusions regarding shape evolution at high spins in ^{69}As and ^{66}Ge are derived from the analysis of the experimental and theoretical transition quadrupole moments—this is a unique case in this mass region. The paper is organized as follows: The experimental setup is described in Sec. II. The lifetime analysis and the experimental results are presented in Sec. III. The results are discussed and compared with the total Routhian surface calculations in Sec. IV, followed by a summary and conclusions in Sec. V.

II. EXPERIMENTAL DETAILS AND DATA ANALYSIS

The ^{69}As and ^{66}Ge nuclei were produced in the reactions $^{40}\text{Ca}(^{32}\text{S}, 3p)^{69}\text{As}$ and $^{40}\text{Ca}(^{32}\text{S}, \alpha 2p)^{66}\text{Ge}$ at a beam energy of 95 MeV. A ^{32}S pulsed beam was delivered from the Tandem XTU accelerator of the INFN Laboratori Nazionali di Legnaro, Legnaro, Italy. The beam, with an intrinsic bunch width of ≈ 1 –2 ns, was pulsed with a 400 ns repetition time.

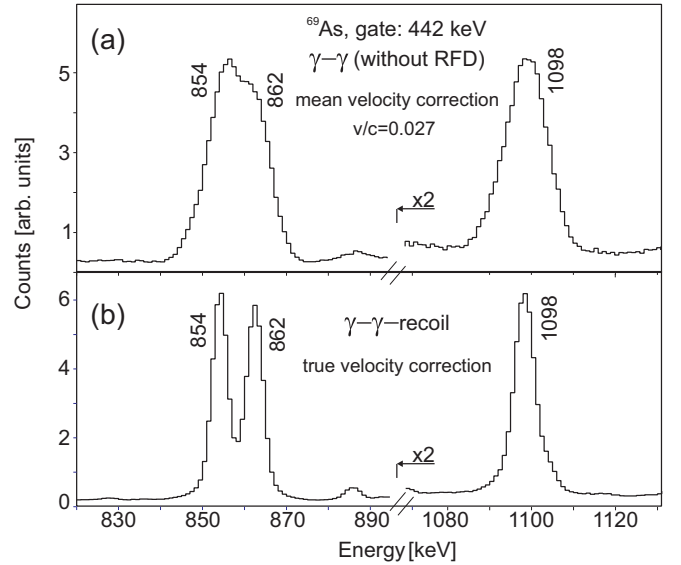


FIG. 1. Part of the coincidence γ -ray spectra from the 95 MeV $^{32}\text{S} + 0.8 \text{ mg/cm}^2 \text{ }^{40}\text{Ca}$ reaction, gated by 442 keV line in ^{69}As . (a) γ - γ spectrum with Doppler correction for the mean recoil velocity ($v/c = 0.027$), (b) γ - γ -recoil spectrum Doppler corrected with the true recoil velocity measured by the RFD. Significant increase in the energy resolution is visible. See text for details.

The target was made of a $0.8 \text{ mg/cm}^2 \text{ }^{40}\text{Ca}$ foil, and to avoid fast oxidation of the target material, it was covered with a $10 \mu\text{g/cm}^2$ carbon layer on both sides.

Deexcitation γ rays from the recoiling reaction products were detected by using the 4π -GASP array [13] consisting of 37 Compton-suppressed HPGGe detectors and, at that time, symmetrically arranged in seven rings located at angles of 35, 60, 72, 90, 108, 120, and 145 degrees with respect to the beam axis. Double- γ coincidence events were stored if they

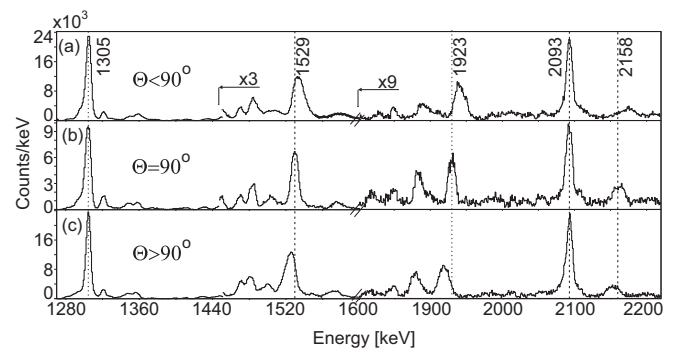


FIG. 2. Double- γ coincidence spectra gated by the ^{69}As transitions (862, 442, 1305, 854, 1098, 1204, 733, and 1177 keV), registered at (a) forward, (b) 90 degree and (c) backward angles with respect to the beam axis. The 1529, 1923, and 2158 keV lines corresponding to the sequential γ transitions in *Band 3* exhibit tails due to very short level lifetimes. For comparison, the sharp γ lines at 1305 and 2093 keV resulting from the levels with longer lifetimes are indicated.

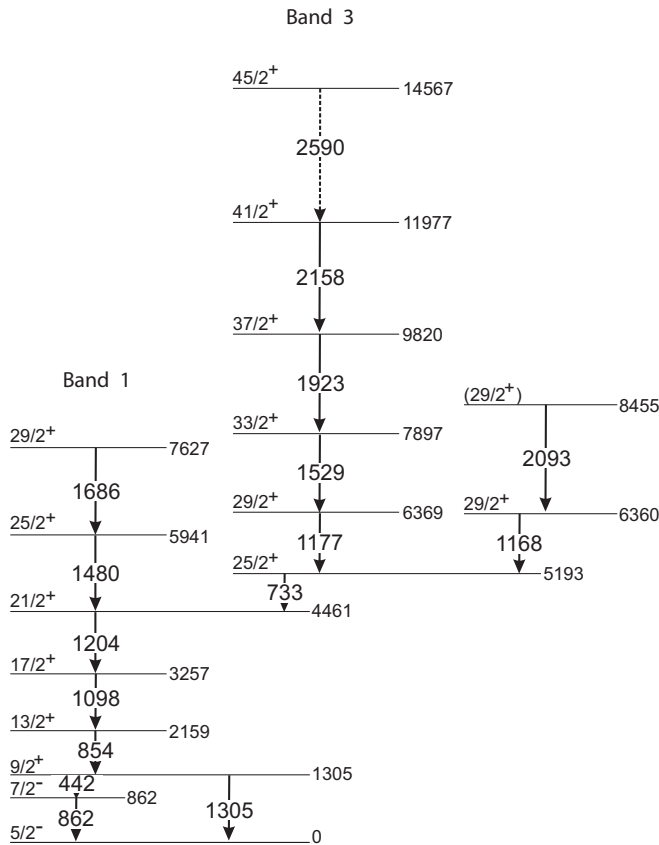


FIG. 3. Partial level scheme of ^{69}As obtained from the 95 MeV $^{32}\text{S} + ^{40}\text{Ca}$ reaction data.

occurred in prompt coincidence with an evaporation residue detected by the recoil filter detector (RFD) [14].

The RFD was placed 1352 mm from the target. Evaporation residues that recoiled out of the thin target into the cone with the aperture of $\theta = 2\text{--}7$ degrees, were registered by 18 ion detectors of the RFD. They were distinguished from scattered projectiles by requiring the following RFD

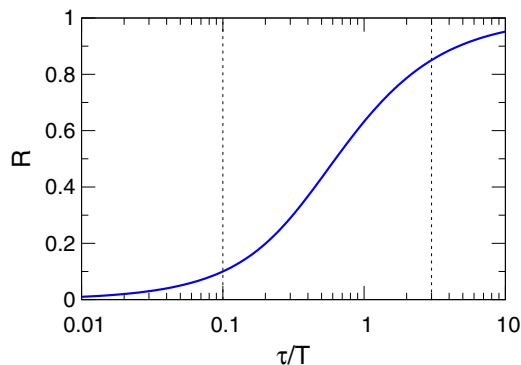


FIG. 4. A fraction of the sharp γ -line component related to the total γ -transition intensity as a function of lifetime τ . The recoil transit time T in the discussed case is estimated to be 600 fs. Dashed vertical lines indicate the limits of the method sensitivity, as described in the text.

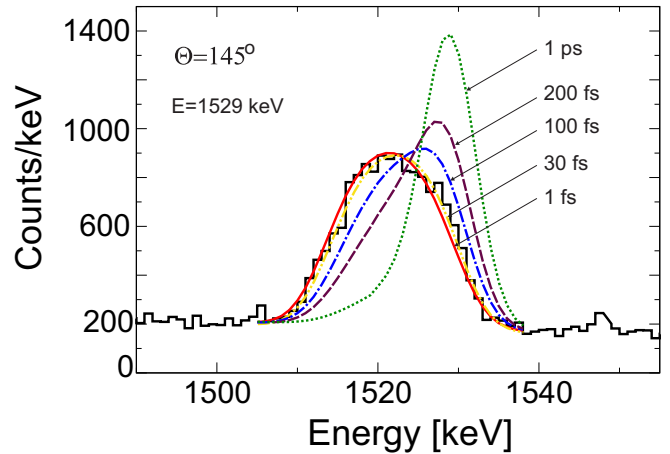


FIG. 5. Comparison of the experimental lineshape for the 1529 keV transition in ^{69}As , registered at the backward angle of 145° with the calculated distributions for several values of τ , from 1 fs to 1 ps. The comparison indicates that the lifetime of the $33/2^+$ state at 7897 keV is of the order of tens of fs. The experimental spectrum was obtained by gating on 733 and 1177 keV transitions in ^{69}As .

conditions, which are specific for the evaporation residues: large signal height, multiplicity $M = 1$, and time of flight with respect to the rf signal $\text{ToF} > 50$ ns.

In the case discussed, the efficiency of the evaporation residue detection was 20%. The position of the single RFD segment that fired provided information on the direction of every individual evaporation residue. In this way the velocity vector of the γ -emitting recoil was reconstructed in the event-by-event mode, allowing for the precise Doppler-shift correction of the γ -ray energy registered in the Ge detectors. As a result, significant improvement in the energy resolution in γ -recoil coincidence spectra has been achieved, as illustrated in Fig. 1. The upper panel [Fig. 1(a)] shows a γ -singles spectrum registered during a short run by the GASP array stand alone, Doppler corrected by using the mean velocity ($v/c = 0.027$) of the recoiling nuclei. The energy resolution in this case is far worse than in the γ -recoil coincidence spectrum presented in Fig. 1(b)—where the Doppler correction was applied for each γ ray by using the measured with RFD velocity vector of the nucleus from which this γ ray was emitted. The energy resolution at $E_\gamma = 1098$ keV is then $\text{FWHM} = 6.8$ keV, compared with $\text{FWHM} = 11.7$ keV when the above mean velocity correction was applied. In Fig. 1(a) one also sees an unresolved double-peak structure for the γ -ray lines at 854 and 862 keV, with the energy resolution of 9.8 keV, whereas in Fig. 1(b) these lines are clearly separated ($\text{FWHM} = 4.9$ keV).

The recoil velocity vector is determined by the RFD at the exit from the target; therefore, the Doppler-shift correction of γ -ray energies is properly accounted only for γ rays emitted after the recoiling nucleus left the target—in such a case the corresponding γ lines are sharp. In contrast, γ lines related to transitions emitted when the recoiling nucleus is still inside the target are Doppler broadened and exhibit a characteristic θ -angle-dependent tail. This is caused by the slowing down and straggling of the recoiling nucleus in the

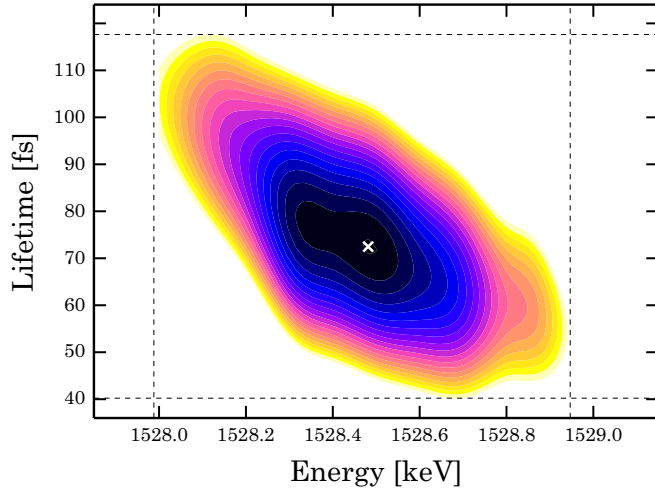


FIG. 6. Two-dimensional χ^2 map for the transition deexciting the $I^\pi = 33/2^+$ state at 7897 keV in ^{69}As , obtained by a simultaneous fit to all detection angles. Minimum is located at $E = 1528.5(-0.5, +0.4)$ keV and $\tau = 72(-32, +45)$ fs. The shown distribution corresponds to the confidence level of 95%, the black dotted lines indicate the uncertainties for the fit parameters.

target. This effect is illustrated in Fig. 2 showing γ spectra of ^{69}As sorted out from the triple γ - γ -recoil coincidence data gated by γ transitions belonging to rotational bands known in this nucleus. As seen in the spectrum (Fig. 2), the applied Doppler correction is appropriate for the 1305 and 2093 keV transitions in ^{69}As , resulting in sharp lines at these energies. In contrast, the 1529, 1923 and 2158 keV lines, which correspond to the sequential transitions in *Band 3* (Fig. 3) known from previous studies [10], are not properly corrected, which indicates that the corresponding γ rays were emitted while the recoiling nucleus was still traveling inside the target. Moreover, these lines do not show any trace of the sharp component, which points to very short lifetimes. This feature allows us to perform the γ -lineshape analysis by means of the Doppler-shift attenuation method (DSAM) in order to extract short lifetimes comparable to or shorter than the recoil nucleus transit time through the target. It can

be shown that the fraction of the nuclei decaying outside the target (giving rise to the sharp γ -line component) related to the total γ transition intensity can be expressed as

$$R = \tau/T[1 - \exp(-T/\tau)], \quad (1)$$

where T is the recoil transit time through the target. The curve shown in Fig. 4 indicates that points corresponding to $R \approx 0.1$, $\tau/T \approx 0.1$, and $R \approx 0.9$, $\tau/T \approx 3$ may set the arbitrary limits of the method sensitivity. In the case described here, the mean transit time of ^{69}As and ^{66}Ge nuclei, calculated by using the SRIM code [15], is 600 fs, therefore the range of lifetimes which could be extracted is 60 fs to 1.8 ps.

In this work, lifetimes of the very short-lived excited states in ^{69}As and ^{66}Ge were extracted by using the γ -ray lineshape analysis method as described in Refs. [14,16]. The method relies on fitting the calculated spectra to the experimental γ -ray lineshapes simultaneously at all angles of detection.

In the model calculations, the attenuation of both the beam in the target and the evaporation residues produced in the reactions occurring along the beam trajectory was considered. Straggling and slowing down of the projectiles and the recoils in the target material were taken into account according to the stopping power tables generated by the SRIM code [15]. For a given τ and transition energy, Doppler-shifted γ -ray spectra were reproduced for all detection angles θ according to the velocity profile $v(t)$ of the recoils. This $v(t)$ distribution resulted from the modeling of the production and stopping processes (for both the projectiles and the residues) in a stack of thin target layers of $\delta x = 10 \mu\text{g}/\text{cm}^2$. A minimization procedure was applied in which the measured γ -ray spectra at different detection angles were taken as input while the lifetime τ and the γ -transition energy E_0 (not determined precisely due to the prompt decay and consequently the excessive Doppler broadening) were considered as fitted parameters. Two-dimensional χ^2 maps were calculated according to the formula

$$\chi^2 = \sum_{i=1}^M [w_i(d_i^{\text{expt}} - d_i^{\text{theor}})]^2, \quad (2)$$

where M denotes total number of points in the spectra used for comparison, d_i^{expt} (d_i^{theor}) are the number of counts in channel

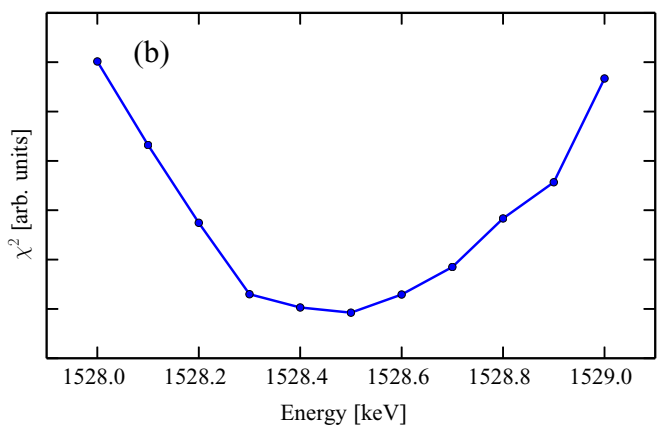
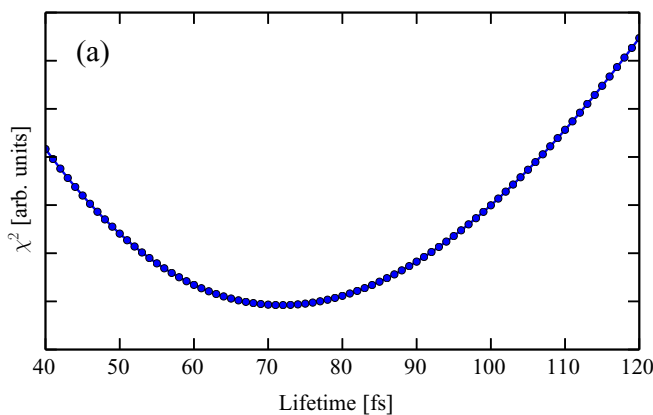


FIG. 7. Projections of the two-dimensional χ^2 distribution, shown in Fig. 6, as a function of (a) lifetime for the optimal transition energy $E = 1528.5$ keV, (b) transition energy for the optimal lifetime $\tau = 72$ fs, for ^{69}As .

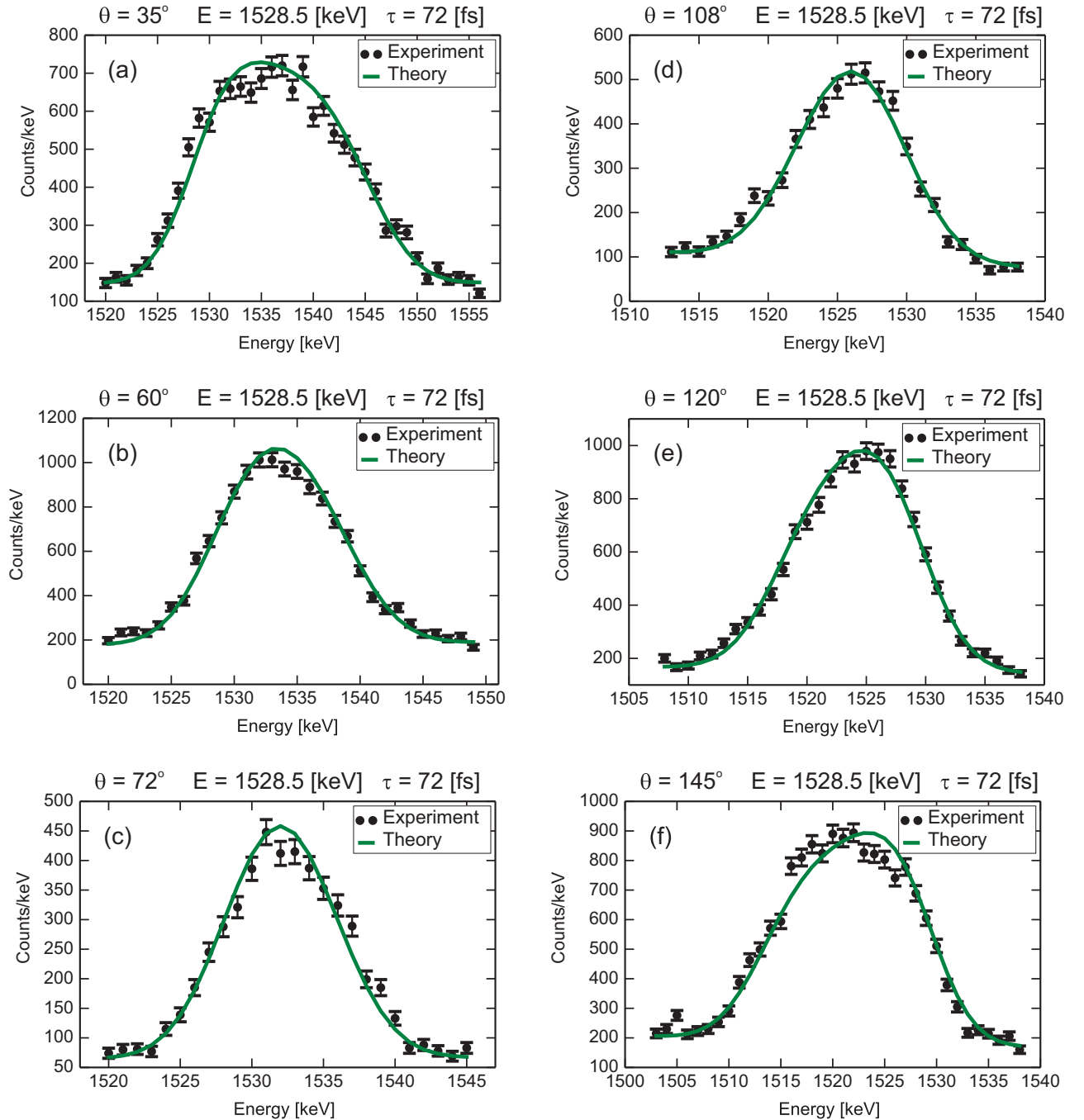


FIG. 8. Comparison between experimental and calculated lineshapes for the 1529 keV transition in ^{69}As seen at all detection angles. The experimental spectra were obtained by gating on the 733 and 1177 keV transitions. The χ^2 minimization resulted in $E = 1528.5$ keV and $\tau = 72$ fs.

i of the experimental (theoretical) spectrum. Experimental points are weighted by the $w_i = (d_i^{\text{expt}})^{-1/2}$ coefficient. The χ^2 minimization provided energy and lifetime values simultaneously. The χ^2 calculations were performed on a dense grid of parameters, the step for the lifetime was 1 fs and 0.1 keV for the γ -ray energy. According to the prescription given in Ref. [17], E_0 and τ uncertainties are determined based on the confidence ellipsoid defined through

$$\chi^2 = \chi_{\min}^2 + g, \quad (3)$$

where the g is the quantile of the χ^2 distribution corresponding to the confidence level of 95%.

III. RESULTS

A. ^{69}As

In ^{69}As , the rotational band labeled as *Band 3* in Ref. [10] and interpreted therein as being built upon a $25/2^+$ state with the $\pi(g_{9/2})^1\nu(g_{9/2})^2$ configuration, was observed in the course of the current experiment up to the spin of $J^\pi = 45/2^+$.

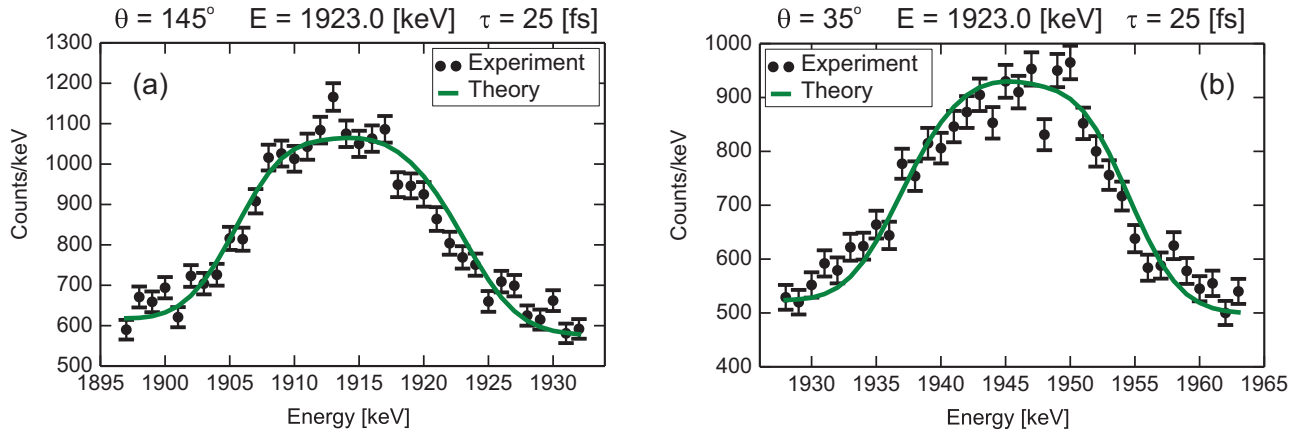


FIG. 9. Comparison between calculated and experimental lineshapes for the 1923 keV transition in ^{69}As detected at (a) $\theta = 145^\circ$ and (b) $\theta = 35^\circ$. The experimental spectra were obtained by gating on the selected ^{69}As transitions, i.e., 862, 442, 1305, 854, 1098, 1204, 733, and 1177 keV. The χ^2 minimization resulted in $E = 1923$ keV and $\tau = 25$ fs. The statistics for this high-spin transition was sufficient to perform a simultaneous fit only for two angles of detection (35° and 145°), therefore the lifetime of the $37/2^+$ state at 9820 keV in ^{69}As is determined as an upper limit of $\tau < 85$ fs; see Fig. 10.

Recorded lineshapes of the in-band transitions (i.e., 1529, 1923, and 2158 keV) suggest that they were all emitted mostly inside the target (Fig. 2), which means that the lifetimes of the decaying states are very short. According to our illustrative analysis, presented in Fig. 5, they are significantly below 100 fs which could confirm the earlier suggestion of superdeformation associated with this band [12].

Complete analysis of the data, taking into account all angles of detection (i.e., 35, 60, 72, 90, 108, 120, and 145 degrees), enabled us to extract the effective lifetime for the $33/2^+$ state at 7897 keV and for the $37/2^+$ state at 9820 keV. In the following manner, Fig. 6 shows the two-dimensional χ^2 surface for the 1529 keV transition deexciting the 7897 keV state, as a result of the simultaneous fit to the spectra collected at all angles of detection. A well-pronounced minimum can be noticed at the energy of 1528.5 ($-0.5, +0.4$) keV and the lifetime of 72 ($-32, +45$) fs for the 7897 keV state. Extracted uncertainties are graphically represented by the contour dotted lines. The one-dimensional sections of the χ^2 surface at the optimal value for individual parameters are illustrated in Fig. 7. In turn, Fig. 8 displays comparison between experimental and calculated lineshapes for the 1529 keV transition for the values obtained in the χ^2 minimum.

The same procedure was applied to the lineshape analysis of the 1923 keV γ -ray transition originating from the $37/2^+$ state at 9820 keV (see Fig. 3); however, the statistics for this high-spin transition was sufficient to perform a simultaneous fit only for two angles of detection, i.e., 35 and 145 degrees. Since these extreme angles are the most sensitive to the lineshape analysis, an upper limit $\tau < 85$ fs for the $37/2^+$ state could be extracted. The outcome of the performed analysis, i.e., a two-dimensional χ^2 surface, a one-dimensional projections of the χ^2 map, and a comparison between experimental and calculated spectra, are presented in Figs. 9–11.

In the analysis, it was assumed that the levels of interest are directly and in-band populated and no unobserved side-feeding effect of a finite lifetime was considered. Thus, the

results are the effective lifetimes which account also for the decay of short-lived higher-lying levels.

In the cases of broad distributions like those for the γ transitions at $E_0 = 1529$ keV and $E_0 = 1923$ keV, which do not contain the stopped component at E_0 , the χ^2 minimization for the individual detection angles do not produce consistent results on lifetimes. This is because the large uncertainty in the transition energy E_0 significantly affects the calculated lineshape. Therefore, in these cases it was crucial to take into account spectra at all the GASP angles simultaneously and perform complex χ^2 minimization in two dimensions (i.e., E_0, τ).

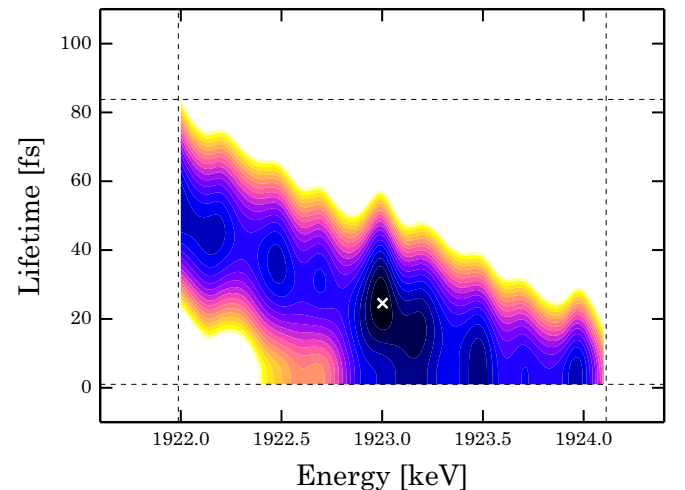


FIG. 10. Two-dimensional χ^2 map for the transition deexciting the $I^\pi = 37/2^+$ state at 9820 keV in ^{69}As , obtained by a simultaneous fit to the spectra registered at $\theta = 35^\circ$ and $\theta = 145^\circ$. Minimum is located at $E = 1923.0(-1.0, +1.1)$ keV and $\tau = 25$ fs. The shown distribution corresponds to the confidence level of 95%, the black dotted lines indicate the uncertainties for the fitted parameters. An upper limit for the 9820 keV level in ^{69}As is $\tau < 85$ fs.

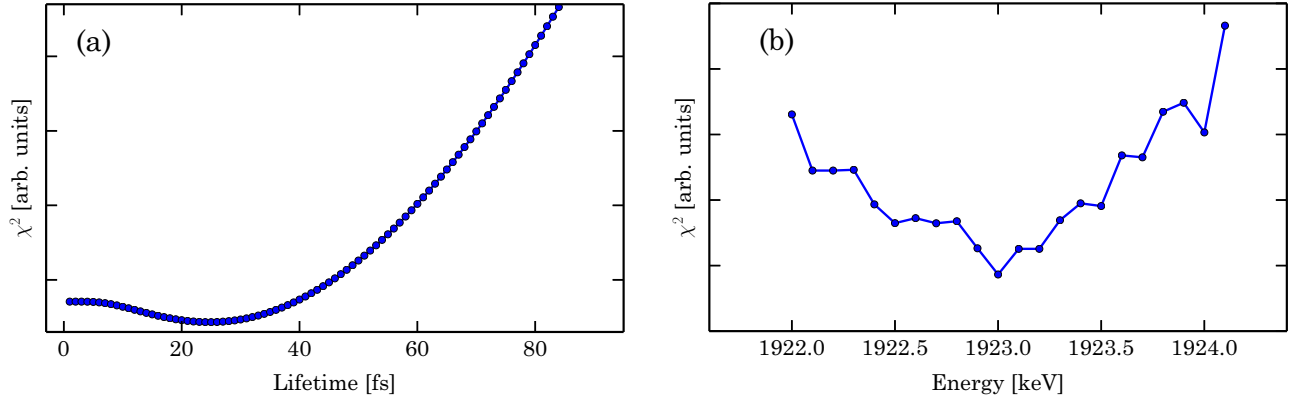


FIG. 11. Projections of the two-dimensional χ^2 distribution shown in Fig. 10 as a function of (a) lifetime for the optimal transition energy $E = 1923.0$ keV, (b) transition energy for the optimal lifetime $\tau = 25$ fs, for ^{69}As .

In this way, we could bring the uncertainty of γ -ray energy determination for the 1529 keV transition down to 0.5 keV, while the literature values vary from 1527.2(4) keV [10] to 1531 keV [12]. Detailed analysis of the lineshape of the 2158 keV transition was impossible due to scarce statistics in the spectra.

The results, i.e., $B(E2)$ transition strengths, lifetimes, and transition energies in ^{69}As , are summarized in Table I. The reduced transition probability $B(E2)$ (listed in Table I) was calculated according to the expressions

$$B(E2, I + 2 \rightarrow I)[e^2 \text{fm}^4] = \frac{8.196 \times 10^{-10}}{E_\gamma^5 [\text{MeV}] \tau [\text{s}]}, \quad (4)$$

$$B(E2)[\text{W.u.}] = \frac{16.8}{A^{4/3}} B(E2)[e^2 \text{fm}^4]. \quad (5)$$

It is worth noting that the lifetimes of the states located above 5193 keV excitation energy in the ^{69}As nucleus have been measured for the first time in the present experiment.

B. ^{66}Ge

In ^{66}Ge , the negative-parity yrast band is known from previous studies [11] up to the spin of 23^- . The γ - γ -recoil coincidence spectra, collected in the current experiment for the three selected rings of GASP detectors, gated by low-lying transitions in coincidence with this band, are presented in Fig. 12. Event-by-event Doppler correction has been applied to the data under the assumption that the γ rays were emitted after the nucleus left the target. As shown in the

TABLE I. Lifetime, γ -ray energy, experimental $B(E2)$ transition strengths in ^{69}As extracted from the present experiment. $B(E2)$ uncertainties correspond to the minimum and maximum lifetimes.

Transition	$33/2^+ \rightarrow 29/2^+$	$37/2^+ \rightarrow 33/2^+$
Energy [keV]	1528.5 (−0.5, +0.4)	1923.0 (−1.0, +1.1)
Lifetime [fs]	72 (−32, +45)	<85
$B(E2)$ [$e^2 \text{fm}^4$]	1364 (−524, +1092)	>370
$B(E2)$ [W.u.]	81 (−31, +65)	>22

Fig. 12, we observe two in-band γ transitions at 1637 and 1969 keV which exhibit large tails due to emission in the target, whereas other transitions belonging to this band seem to be narrow, therefore associated with longer lifetimes. The collected statistics allowed us to apply the lineshape analysis only for the 1637 keV transition to extract the lifetime of the $I^\pi = 11^-$ state at 7130 keV.

The lineshape analysis of the 1637 keV transition yielded the effective lifetime of 250 ± 50 fs for this state and has already been reported in Ref. [5]. A more detailed analysis of the feeding to that state allowed us to extract its lifetime. It was noticed that γ rays of 506, 607, 717, and 1413 keV, feeding the $I^\pi = 11^-$ state at 7130 keV (see Fig. 13), did not show any traces of shifted components at any angle,

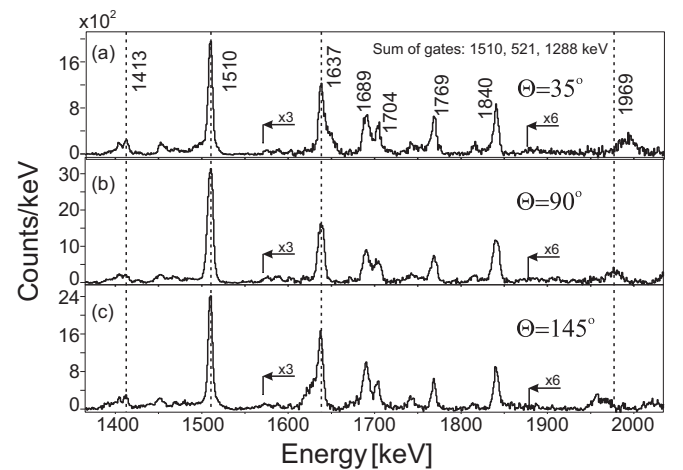


FIG. 12. The summed spectra of γ rays gated on the 1510, 521, and 1288 keV transitions of the negative-parity rotational band in ^{66}Ge . The upper panel (a) shows γ rays registered at forward angle $\theta = 35^\circ$, the middle panel (b) corresponds to $\theta = 90^\circ$, and the lowest panel (c) shows those detected at the backward angle $\theta = 145^\circ$ with respect to the beam axis. The 1637 and 1969 keV lines, corresponding to the coincident γ transitions, exhibit angle-dependent tails due to lifetimes in femtosecond range. In contrast, the sharp γ line visible at 1510 keV results from gamma decay of a long-lived state.

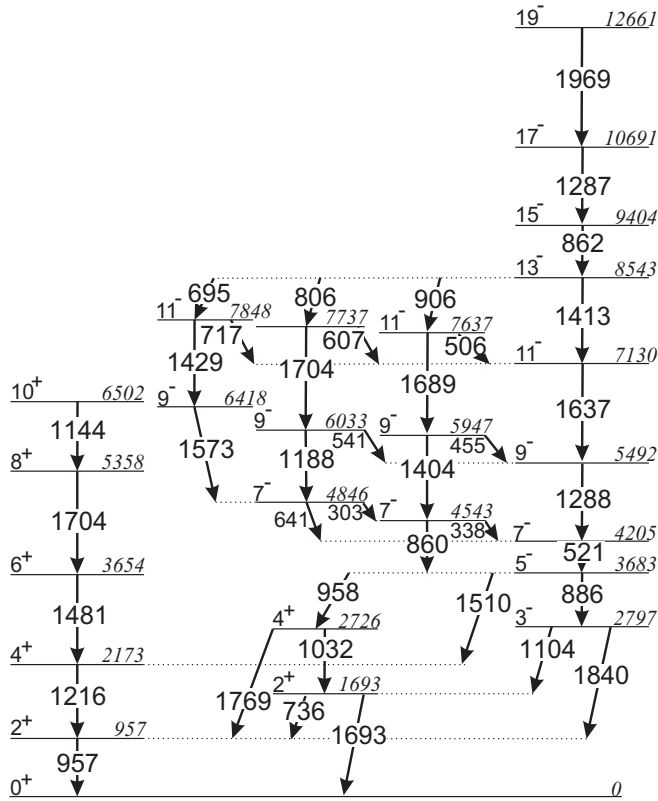


FIG. 13. Partial level scheme of ^{66}Ge obtained from the 95 MeV $^{32}\text{S} + ^{40}\text{Ca}$ reaction data.

which indicates lifetimes of states deexcited by those γ rays longer than the recoil transit time through the target. Gates set on those long-lived transitions, above the level of interest, yielded spectra which we subtracted from the initial spectrum presented in Fig. 12 (the efficiency of the GASP germanium array was taken into account). Resulting spectra for forward and backward angles are presented in Fig. 14. Owing to that procedure we could exclude the effect of feeding from the known long-lived states above the measured 11^- state of interest. Contribution to the lifetime from unobserved transitions is assumed to be very small, thus this effect was not

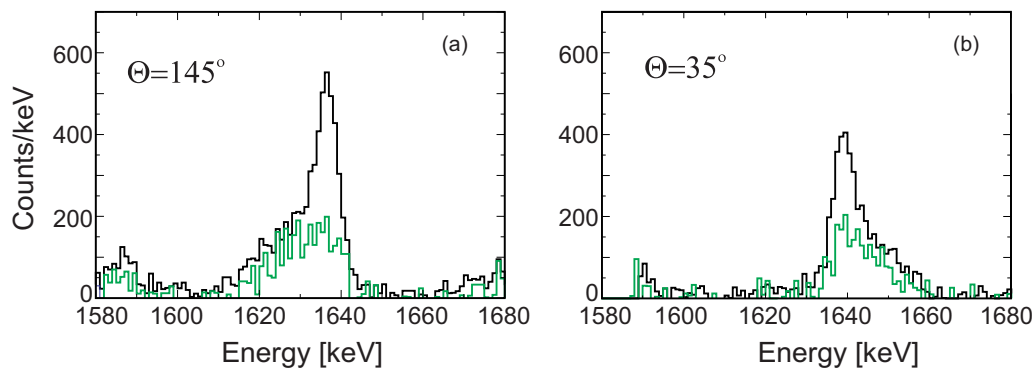


FIG. 14. Line shape of the 1637 keV transition in ^{66}Ge seen at (a) the backward angle $\theta = 145^\circ$ and (b) the forward angle $\theta = 35^\circ$. The black line shows part of the spectrum shown in Fig. 12, the green (light gray) line shows the spectrum obtained after subtraction of the side feeding by the 506, 607, 717, and 1413 keV transitions. For more details see explanation in text.

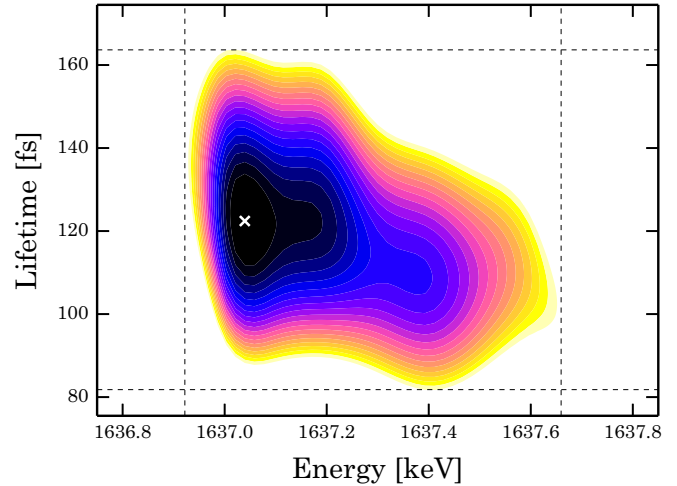


FIG. 15. Two-dimensional χ^2 map for the transition deexciting the $I^\pi = 11^-$ state at 7130 keV in ^{66}Ge , obtained by a simultaneous fit to the spectra registered at $\theta = 35^\circ$, $\theta = 90^\circ$, and $\theta = 145^\circ$. Minimum is located at $E = 1637.1(-0.2, +0.5)$ keV and $\tau = 122 (\pm 41)$ fs. The distribution shown corresponds to the confidence level of 95%, the black dotted lines indicate the uncertainties for the fitted parameters.

considered in the analysis. A simultaneous fit of the spectra registered at 35° , 90° , and 145° after subtracting the long-lived components yielded the two-dimensional χ^2 surface, shown in Fig. 15, and its projections in Fig. 16. The χ^2 minimization resulted in the lifetime of $\tau = 122 (\pm 41)$ fs for the $I^\pi = 11^-$ state at 7130 keV in ^{66}Ge that gives the reduced transition probability $B(E2) = 569 (\pm 191) e^2 \text{ fm}^4$, according to Eq. (4). Experimental spectra together with the calculated lineshapes for the values arising from χ^2 surface minimization for the 1637 keV transition are shown in Fig. 17.

Experimental information on ^{66}Ge obtained from present measurement is summarized in Table II.

IV. DISCUSSION

The measured lifetimes of the excited states can provide reduced transition probabilities between the excited states,

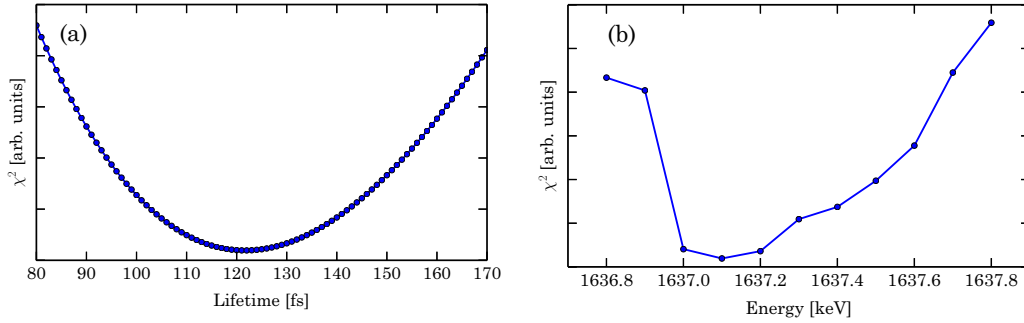


FIG. 16. Projections of the two-dimensional χ^2 distribution, shown in Fig. 15, as a function of (a) lifetime for the optimal transition energy $E = 1637.1$ keV, (b) transition energy for the optimal lifetime $\tau = 122$ fs, for ^{66}Ge .

which in the case of a rotational band, allow us to extract the transition quadrupole moments Q_t and hence to deduce the nuclear deformation. The transition probability T [s^{-1}] for a band member of a spin I is described by the expression [18]

$$T(E2, I + 2 \rightarrow I) = 1.22 \times 10^9 E_\gamma^5 [\text{MeV}] B(E2) [e^2 \text{fm}^4], \quad (6)$$

where the reduced transition probability $B(E2)$ is given by

$$B(E2, I + 2 \rightarrow I) = \frac{5}{16\pi} Q_t^2 (I + 2K)(I + 2K)^2. \quad (7)$$

The K value is the projection of the total spin I onto the symmetry axis of the deformed nucleus. After inserting the Clebsch-Gordan ($|C_K^{I+2} \frac{2}{0} I_K|$) coefficients, $B(E2)$ can be related to the transition quadrupole moment Q_t via the formula

$$B(E2, I + 2 \rightarrow I) = \frac{5}{16\pi} Q_t^2 \frac{3}{2} \times \frac{(I + 1 - K)(I + 1 + K)(I + 2 - K)(I + 2 + K)}{(I + 1)(2I + 3)(I + 2)(2I + 5)}. \quad (8)$$

For an axial nucleus, the intrinsic quadrupole moment Q_{20} defined in the body-fixed frame, and the transition quadrupole

moment Q_t [derived from the reduced transition probability $B(E2)$] are equal and related to the quadrupole deformation β_2 via the equation

$$Q_t = Q_{20} = \frac{3}{\sqrt{5\pi}} Z e R_0^2 \beta_2. \quad (9)$$

When the axial symmetry breaks and the nuclear shape becomes triaxial, the intrinsic quadrupole moment Q_0 and the transition quadrupole moment Q_t are related to the deformation parameters β_2 and γ via equations [19,20]

$$Q_0 = Q_{20}(\gamma = 0^\circ) \frac{\sin(\gamma + 30^\circ)}{\sin 30^\circ}, \quad (10)$$

$$Q_t = Q_{20}(\gamma = 0^\circ) \frac{\cos(\gamma + 30^\circ)}{\cos 30^\circ}, \quad (11)$$

where $Q_{20}(\gamma = 0^\circ)$ can be calculated by using Eq. (9).

The intrinsic quadrupole moment Q_0 is specific for a single state, while the transition quadrupole moment Q_t probes the geometry of the initial and the final states whose wave functions might correspond to very different configurations. Within a given band Q_0 and Q_t , moments usually have different values, which might also vary with angular momentum.

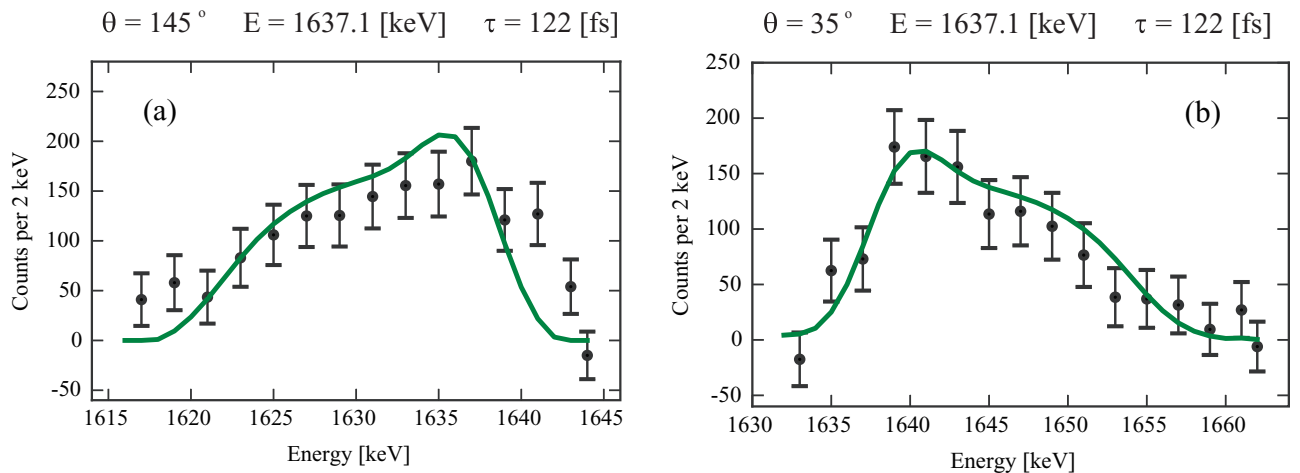


FIG. 17. Comparison between experimental and calculated lineshapes seen at (a) $\theta = 145^\circ$ and (b) $\theta = 35^\circ$ detection angles for the transition deexciting the $I^\pi = 11^-$ state at 7130 keV in ^{66}Ge , assuming the χ_{min}^2 energy and lifetime values. Experimental spectra were obtained by gating on the 521, 1288, and 1510 keV transitions and side feeding subtraction. For more details see explanation in text.

TABLE II. Lifetime, γ -ray energy, experimental $B(E2)$ transition strength in ^{66}Ge extracted from the present experiment. $B(E2)$ uncertainties correspond to the minimum and maximum lifetimes.

Transition $I_i \rightarrow I_f$	$11^- \rightarrow 9^-$
Energy [keV]	1637.1 (-0.2, +0.5)
Lifetime [fs]	122 (± 41)
$B(E2)$ [$e^2 \text{fm}^4$]	571 (-143, +289)
$B(E2)$ [W.u.]	36 (-9, +18)

When Q_0 and Q_t are close, the static-rotor model assumption is fulfilled which means that one deals with a well-deformed rotational band that is not mixed with other bands.

A. ^{69}As

To describe the spectroscopic properties of the studied nuclei, the cranked Woods-Saxon-Strutinsky calculations by means of TRS method [4] were performed. The ^{69}As nucleus has 33 protons and 36 neutrons, i.e., one valence proton and four neutrons above the spherical gap at $N = Z = 32$. In this theoretical approach, a single proton occupying the $g_{9/2}$ orbit was blocked. The set of potential-energy surface maps presented in Fig. 18 illustrates the deformation and the shape evolution with increasing rotational frequency for this configuration in ^{69}As .

According to the calculations, at low rotational frequencies ($\hbar\omega$ up to 0.8 MeV) the deepest minimum of the

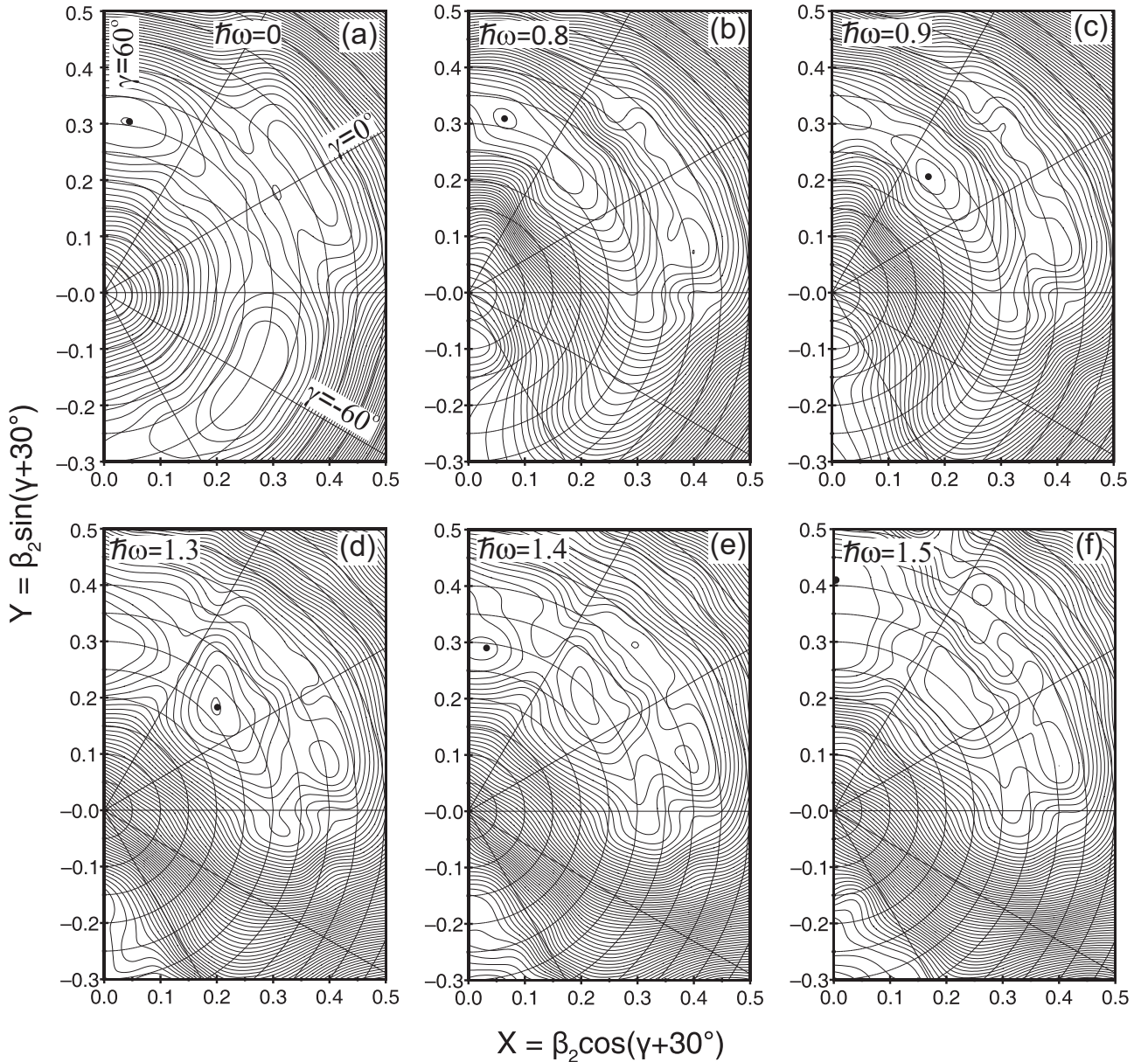


FIG. 18. Total Routhian surfaces for positive-parity $\alpha = 1/2$ states in ^{69}As at (a) $\hbar\omega = 0$ MeV, (b) $\hbar\omega = 0.8$ MeV, (c) $\hbar\omega = 0.9$ MeV, (d) $\hbar\omega = 1.3$ MeV, (e) $\hbar\omega = 1.4$ MeV, and (f) $\hbar\omega = 1.5$ MeV. The black dot indicates the lowest minimum. The energy difference between neighboring equipotential lines is 200 keV. The minima are located at (a) $\beta_2 = 0.31$, $\gamma = 52^\circ$, (b) $\beta_2 = 0.32$, $\gamma = 48^\circ$, (c) $\beta_2 = 0.27$, $\gamma = 20^\circ$, (d) $\beta_2 = 0.27$, $\gamma = 12^\circ$, (e) $\beta_2 = 0.29$, $\gamma = 54^\circ$, and (f) $\beta_2 = 0.4$, $\gamma = 60^\circ$.

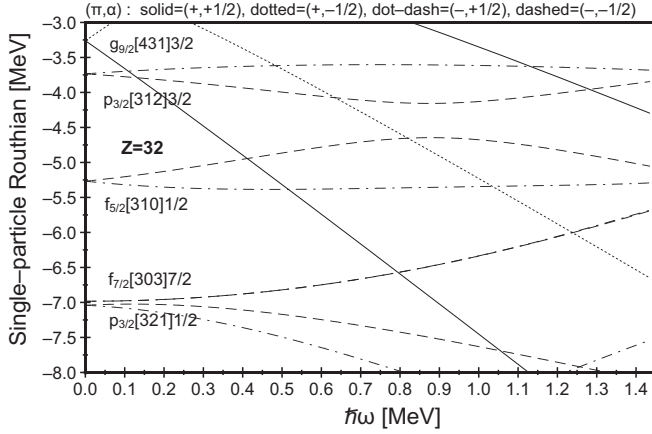


FIG. 19. Woods-Saxon proton single-particle Routhians versus rotational frequency (for $\beta_2 = 0.27$, $\gamma = 20^\circ$) for ^{69}As , the unpaired proton is located on the $g_{9/2}$ orbital, with $K = 3/2$.

potential-energy surface is located at the oblate noncollective shape with $\beta_2 \approx 0.3$ and $\gamma \approx 50^\circ$ [Figs. 18(a) and 18(b)]. However, as the rotational frequency increases the ^{69}As nucleus becomes triaxial prolate, e.g., when $\hbar\omega$ reaches the value of 0.9 MeV, the absolute minimum moves from the noncollective oblate to the prolate-deformed collective shape with $\beta_2 \approx 0.27$ and $\gamma \approx 20^\circ$ [Fig. 18(c)]. This shape remains dominant up to $\hbar\omega = 1.3$ MeV [Fig. 18(d)], afterwards the nucleus surface returns to the primary noncollective oblate shape [Fig. 18(e)]. A further increase of the rotational frequency reveals vanishing of the triaxiality [Fig. 18(f)]—from $\hbar\omega = 1.5$ MeV the shape becomes noncollective oblate with $\beta_2 \approx 0.4$ and $\gamma \approx 60^\circ$.

Experimentally, it is difficult to determine the value of the triaxial parameter γ for a nucleus. When the axial symmetry breaks, one cannot determine the quadrupole deformation parameters (β_2 and γ) at the same time from the experimental $B(E2)$ value. Therefore, in the following discussion we focus on a transition quadrupole moment comparison.

The extracted lifetimes were used to calculate transition quadrupole moments Q_t for the $33/2^+$ state at 7897 keV and the lower limit for the $37/2^+$ state at 9820 keV. According to the plot of single-particle Routhians (presented in Fig. 19) the unpaired proton is located in the $g_{9/2}$ [431] orbital, with $K = 3/2$, therefore this K quantum number was used in Eq. (7) for calculations of the experimental Q_t . The obtained values (listed in Table III) are $|Q_t(K = 3/2)| =$

1.99 (−0.43, +0.68) eb for the $33/2^+$ state and the lower limit for the $37/2^+$ state as $|Q_t(K = 3/2)| > 1.03$ eb.

The obtained quadrupole moments for the states of *Band 3* in ^{69}As , which were discussed above, can be compared with those predicted by TRS calculations. The sequence of collective prolate-deformed states (for $\hbar\omega$ between 0.9 and 1.3 MeV) corresponds to the theoretical excitation energies ranging from 6905 keV up to the 13284 keV, and spins from $29/2^+$ to $45/2^+$, which matches well the energies and spins of states for which lifetimes were determined in this work. These theoretical calculations reproduce quite well the experimental *Band 3* level energies. Also, the quadrupole moment, calculated from the measured lifetimes to be $|Q_t(K = 3/2)| = 1.99$ (−0.43, +0.68) eb for the $33/2^+$ state and the lower limit for the $37/2^+$ state as $|Q_t(K = 3/2)| > 1.03$ eb, agree with the results of calculations (see Table III). This indicates that *Band 3* in ^{69}As at the spin of $33/2^+$ exhibits a transition to the collective regime and above this angular momentum can be attributed to the prolate-deformed collective structure with $\beta_2 \approx 0.27$ and $\gamma \approx 20^\circ$ although, one should be aware of the rotor model approximation made for the experimental Q_t extraction.

The obtained results are clearly in line with the predicted shape evolution scenario in this nucleus which shows a shape change from the noncollective oblate to prolate-deformed collective one.

Another feature that is apparent in the presented TRS calculations is that, at low rotational frequency, the potential-energy surface shows also the existence of a prolate-deformed collective minimum with $\beta_2 \approx 0.4$ and $\gamma \approx -20^\circ$ [Fig. 18(a)]. This prolate-deformed structure exists up to very high rotational frequency ($\hbar\omega = 1.4$ MeV) and, when comparing its energy-spin dependence, it could also correspond to *Band 3* in ^{69}As . However, the transition quadrupole moment of this calculated collective band, $Q_t = 3.62$ eb, exceeds significantly the experimental value of 1.99 (−0.43, +0.68) eb, which rather excludes such assignment. In the TRS map seen in Fig. 18(a) there is another collective oblate minimum with $\beta_2 \approx 0.3$ and $\gamma \approx -50^\circ$ which exists up to $\hbar\omega = 0.5$ MeV. This structure may correspond to the positive yrast band (*Band 1*) in ^{69}As (see Fig. 3) that seems to terminate at higher rotational frequencies [10].

B. ^{66}Ge

The shape evolution in ^{66}Ge nucleus ($N = 34$, $Z = 32$) with two neutrons outside the $N = Z$ line was studied

TABLE III. Comparison of experimental Q_t values with theoretical ones calculated at different rotational frequencies for the yrast band in ^{69}As .

Theoretical			Experimental		
$\hbar\omega$ [MeV]	(β_2, γ)	Q_t [eb]	$\hbar\omega$ [MeV]	E_γ [keV]	$ Q_t(K = 3/2) $ [eb]
0.7	(0.315, 48)	−1.96			
0.8	(0.316, 48)	−1.96	0.76	1528.5	1.99 (−0.43, +0.68)
0.9	(0.268, 20)	1.42	0.96	1923.0	>1.03
1.0	(0.267, 20)	1.40			

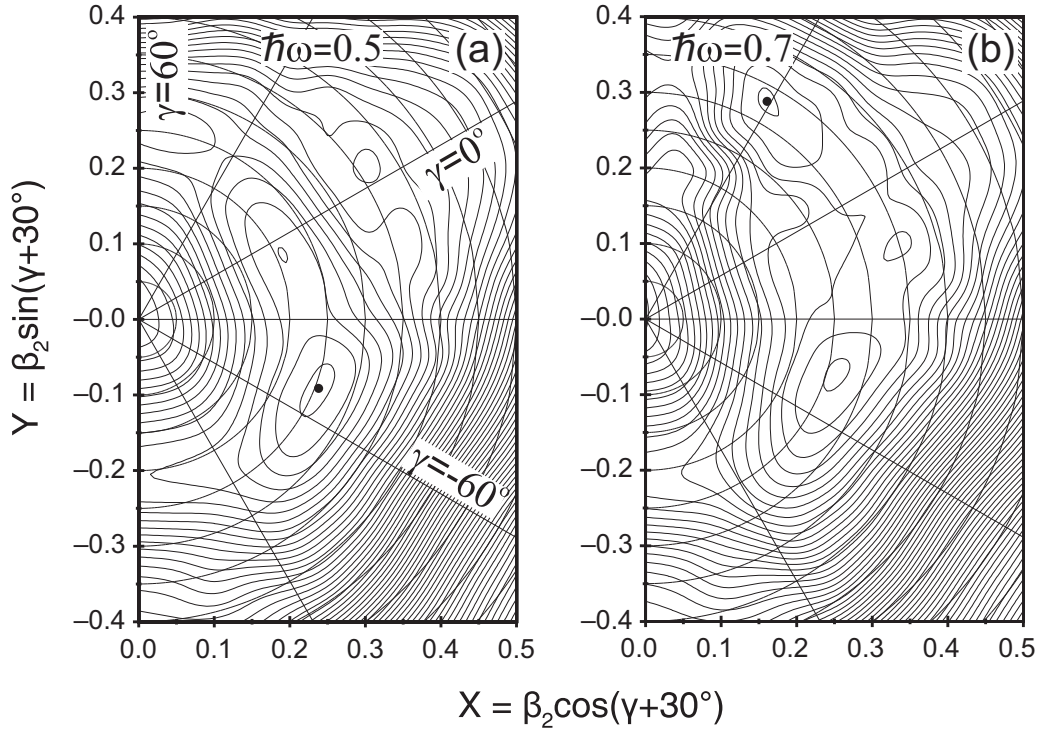


FIG. 20. Total Routhian surfaces at (a) $\hbar\omega = 0.5$ MeV and (b) $\hbar\omega = 0.7$ MeV for ^{66}Ge . The minima are located at (a) $\beta_2 = 0.26$, $\gamma = -51^\circ$ —collective oblate minimum—and (b) $\beta_2 = 0.33$, $\gamma = 31^\circ$ —triaxial prolate minimum.

theoretically by calculating the TRS surfaces at different rotational frequencies. For this nucleus, the energy potential surfaces present the shape change from the collective oblate to the triaxial prolate—the opposite situation when comparing with the ^{69}As case, as described earlier in this paper. For low rotational frequencies the predicted shape is collective oblate with $\beta_2 = 0.26$ and $\gamma = -51^\circ$ [see Fig. 20(a)]. When $\hbar\omega$ reaches a value of 0.7 MeV, the absolute minimum moves from the collective oblate to the triaxial prolate structure built on the 7^- state at 4205 keV with $\beta_2 = 0.33$ and $\gamma = 31^\circ$

[Fig. 20(b)]. This shape remains dominant until a very high value of rotational frequency.

From the proton single-particle Routhian plot [Fig. 21(a)], in the ground state, no particles are occupied in the $g_{9/2}$ orbital [notice the $Z = 30$ gap in the single-particle Routhian picture, the $Z = 32$ gap should be located between the $f_{5/2}([303]5/2)$ and $g_{9/2}([404]9/2)$ orbitals]. For the rotational frequency $\hbar\omega \approx 0.7$ MeV single-proton orbitals, $g_{9/2}([404]9/2)$ and $f_{5/2}([303]5/2)$ cross, resulting in a particle in $g_{9/2}([404]9/2)$ and a hole in $f_{5/2}([303]5/2)$, this configuration couples to

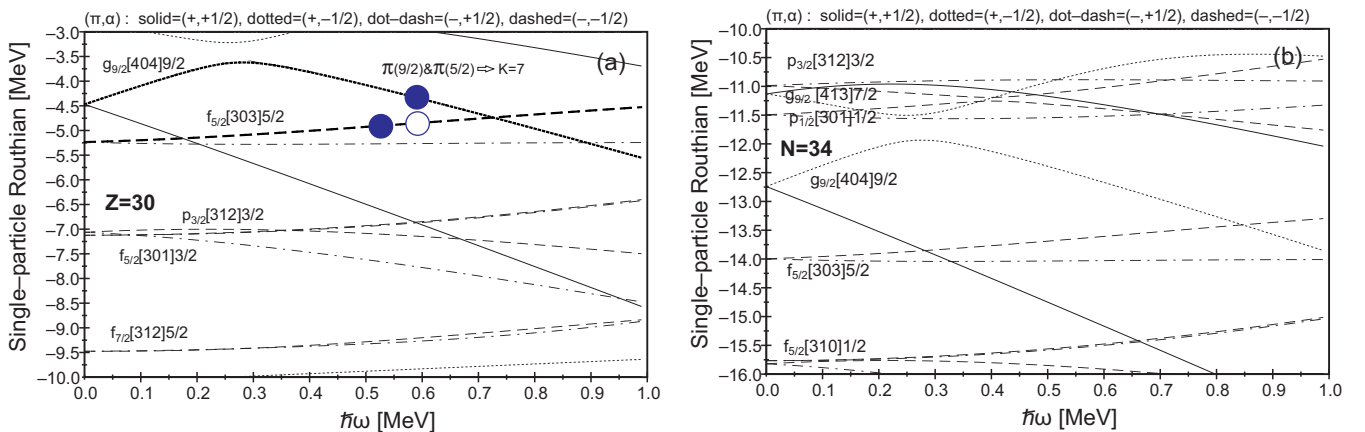


FIG. 21. Woods-Saxon (a) proton and (b) neutron single-particle Routhians calculated versus rotational frequency (for $\beta_2 = 0.33$ and $\gamma = 30^\circ$) for ^{66}Ge . For the rotational frequency $\hbar\omega \approx 0.7$ MeV single proton orbitals: $g_{9/2}([404]9/2)$ and $f_{5/2}([303]5/2)$ crosses, this configuration couples to a spin of 7^- .

TABLE IV. Comparison of the experimental Q_t values and the theoretical ones calculated at different rotational frequencies for the yrast band in ^{66}Ge .

Theoretical			Experimental		
$\hbar\omega$ [MeV]	(β_2, γ)	Q_t [eb]	$\hbar\omega$ [MeV]	E_γ [keV]	$ Q_t(K=7) $ [eb]
0.5	(0.255, -51)	-1.74			
0.6	(0.259, -48)	-1.78			
0.7	(0.328, 30)	-2.48			
0.8	(0.323, 30)	-2.50	0.82	1637.1	2.35 (-0.31, +0.54)

the spin 7^- . However, there is no sign of a neutron orbital crossing near the Fermi level [Fig. 21(b)]. This means that the spin of the bandhead can be assigned as 7^- —therefore, the $K=7$ value was used in the further experimental Q_t calculations.

The 1637 keV transition deexciting the 11^- state at 7130 keV in ^{66}Ge , for which the excited-state lifetime was determined in this work, is in the range of rotational frequencies where the nucleus should take a triaxial shape according to the TRS calculations. The experimental transition quadrupole moment [resulting from the measured lifetime of $122 (\pm 41)$ fs for 1637 keV line] equals $|Q_t(K=7)| = 2.35 (-0.31, +0.54)$ eb and is in very good agreement with the theoretical Q_t value of -2.50 eb (see Table IV).

In ^{66}Ge , several 11^- levels are close together and enhanced $B(E2)$ might suggest the band crossing and mixing of configurations associated with different β_2 and γ deformations. This effect can be seen through the TRS-determined deformation that is $\hbar\omega$ dependent. Different statuses of band crossing and configuration mixing lead to different deformations, as one can see, for example, in the band crossing discussed at $\hbar\omega \approx 0.7$ MeV in Fig. 21.

V. CONCLUSIONS

To summarize, the femtosecond-range lifetimes of excited states in ^{69}As and ^{66}Ge were assessed for the first time by measuring γ -recoil coincidences with the GASP germanium array and the recoil filter detector. Analysis of the 1529 keV γ lineshape in ^{69}As allowed us to extract the lifetime $\tau = 72 (-32, +45)$ fs for the $I^\pi = 33/2^+$ state at 7897 keV and the resulting transition quadrupole moment $|Q_t(K=3/2)| = 1.99 (-0.43, +0.68)$ eb; it also provided the lower limit $|Q_t(K=3/2)| > 1.03$ eb for the $37/2^+$ state.

TRS calculations were performed to interpret the experimental results on the basis of the coexisting rotational

collective structures. In ^{69}As , the calculations predict two positive-parity collective structures which might be associated with the experimental *Band 3*. Our result for the transition quadrupole moment enabled us to constrain the assignment of *Band 3* as the yrast structure that becomes prolate deformed with rather moderate deformation $\beta_2 \approx 0.27$ and $\gamma \approx 20^\circ$. This gives support for the scenario of a shape change from the noncollective oblate- to prolate-deformed collective one, as predicted by the TRS.

Analysis of the 1637 keV γ lineshape allowed us to extract the lifetime $\tau = 122 (\pm 41)$ fs for the $I^\pi = 11^-$ state at 7130 keV in ^{66}Ge , from which the transition quadrupole moment of the negative-parity band built on the 7^- state at 4205 keV could be deduced. This is in line with the TRS calculations, according to which the shape of ^{66}Ge changes from the collective oblate at low rotational frequency to the triaxial prolate at higher rotational frequencies—the opposite situation with respect to the ^{69}As case.

Such opposite behavior of shape evolution with spin in the neighboring nuclei ^{66}Ge and ^{69}As illustrates a delicate interplay of the nucleons above $N=Z=32$, resulting in driving the nucleus toward different shapes, and points to the importance of the unpaired $g_{9/2}$ proton in stabilizing the collectivity in ^{69}As at a moderate rotation frequency.

In the final note, it should be mentioned that very short lifetimes measured in these shape-transitional nuclei, which might indicate a high degree of β_2 deformation, indeed correspond rather to moderate elongation but significant triaxiality in terms of the γ -deformation parameter.

ACKNOWLEDGMENTS

This work was supported by the National Science Center (NCN), Poland under HARMONIA Contract No. 2013/08/M/ST2/00591. F.R.X. and W.Y.L. acknowledge support from the Natural Science Foundation of China under Grant No. 11835001.

- [1] W. Nazarewicz *et al.*, Microscopic study of the high-spin behaviour in selected $A \simeq 80$ nuclei, *Nucl. Phys. A* **435**, 397 (1985).
 [2] M. Hasegawa *et al.*, Phase transition in exotic nuclei along the $N=Z$ line, *Phys. Lett. B* **656**, 51 (2007).

- [3] K. Nomura, R. Rodriguez-Guzman, and L. M. Robledo, Structural evolution in germanium and selenium nuclei within the mapped interacting boson model based on the Gogny energy density functional, *Phys. Rev. C* **95**, 064310 (2017).

- [4] F. R. Xu, W. Satuła, and R. Wyss, Quadrupole pairing interaction and signature inversion, *Nucl. Phys. A* **669**, 119 (2000).
- [5] M. Matejska-Minda *et al.*, Lifetime measurement of short-lived states in ^{66}Ge , *Acta Phys. Pol., B* **44**, 501 (2013).
- [6] M. Matejska-Minda *et al.*, Lifetime measurement of short-lived states in ^{69}As , *Acta Phys. Pol., B* **45**, 235 (2014).
- [7] S. S. Bhattacharjee *et al.*, Shape evolution with increasing angular momentum in the ^{66}Ge nucleus, *Phys. Rev. C* **95**, 054330 (2017).
- [8] J. J. Sun *et al.*, Band crossing and shape evolution in ^{73}Ge , *Phys. Rev. C* **92**, 054302 (2015).
- [9] A. Corsi *et al.*, Collectivity of light Ge and As isotopes, *Phys. Rev. C* **88**, 044311 (2013).
- [10] I. Stefanescu *et al.*, High-spin states and band terminations in ^{69}As , *Phys. Rev. C* **70**, 044304 (2004).
- [11] E. A. Stefanova *et al.*, Four-quasiparticle alignments in ^{66}Ge , *Phys. Rev. C* **67**, 054319 (2003).
- [12] A. M. Bruce *et al.*, Two-neutron alignment and shape changes in ^{69}As , *Phys. Rev. C* **62**, 027303 (2000).
- [13] C. Rossi Alvarez, The GASP array, *Nucl. Phys. News* **3**, 10 (1993).
- [14] W. Męczyński *et al.*, A detector for filtering γ -ray spectra from weak fusion-evaporation reactions out of strong background and for Doppler correction: The recoil filter detector, RFD, *Nucl. Instrum. Methods Phys. Res., Sect. A* **580**, 1310 (2007).
- [15] <http://www.srim.org/>
- [16] P. Bednarczyk *et al.*, High spin structure study of the light Odd-A $f_{7/2}$ nuclei: ^{45}Sc , ^{45}Ti and ^{43}Ca , *Eur. Phys. J. A* **2**, 157 (1998).
- [17] S. Brandt, *Statistical and Computational Methods in Data Analysis* (Springer, New York, 1997).
- [18] H. Morinaga and T. Yamazaki, *In-Beam Gamma-Ray Spectroscopy* (North-Holland, Amsterdam, 1976).
- [19] D. N. Poenaru and W. Greiner, *Handbook of Nuclear Properties* (Oxford University Press, Clarendon Press, Oxford, 1996).
- [20] F. Brandolini, Rotational bands and alignments in the $1f_{7/2}$ shell, *Eur. Phys. J. A* **20**, 139 (2004).